J. Fluid Mech. (2015), *vol.* 785, *pp.* 301–323. © Cambridge University Press 2015
doi:10.1017/jfm.2015.627

A new inviscid mode of instability in compressible boundary-layer flows

Adam P. Tunney[1,†], James P. Denier[2], Trent W. Mattner[3] and John E. Cater[1]

[1]Department of Engineering Science, University of Auckland, Auckland 1142, New Zealand

[2]Department of Mathematics, Macquarie University, Sydney, NSW 2109, Australia

[3]School of Mathematical Sciences, University of Adelaide, Adelaide, SA 5005, Australia

(Received 28 February 2015; revised 20 October 2015; accepted 21 October 2015;
first published online 23 November 2015)

The stability of an almost inviscid compressible fluid flowing over a rigid heated surface is considered. We focus on the boundary layer that arises. The effect of surface heating is known to induce a streamwise acceleration in the boundary layer near the surface. This manifests in a streamwise velocity which exhibits a maximum larger than the free-stream velocity (i.e. the streamwise velocity exhibits an 'overshoot' region). We explore the impact of this overshoot on the stability of the boundary layer, demonstrating that the compressible form of the classical Rayleigh equation (which governs the development of short wavelength instabilities) possesses a new unstable mode that is a direct consequence of this overshoot. The structure of this new class of modes in the small wavenumber limit is detailed, providing a valuable confirmation of our numerical results obtained from the full inviscid eigenvalue problem.

Key words: boundary layer stability, compressible boundary layers, high-speed flow

1. Introduction

Various paths of transition from laminar to turbulent flow have been identified (Morkovin & Reshotko 1990) that depend sensitively on the relative size of the disturbance to the laminar flow. In low-disturbance environments, such as aerodynamic flight, the transition process in the boundary layer over a body generally proceeds via a sequence of receptivity, linear growth and nonlinear breakdown. Receptivity is the process through which disturbances, either in the form of free-stream turbulence, wall roughness or acoustic sources, are internalised into the flow. Provided that the disturbance is small in the boundary layer, the initial growth or decay of the disturbance can often be adequately modelled by linear stability theory. Unstable disturbances grow rapidly until nonlinear effects become dominant, and subsequent secondary instabilities can then arise that induce the cascade to the smaller scales that are the characteristic of many turbulent flows (for example see Schmid & Henningson 2001).

The work of Lees & Lin (1946) initiated the extension of linear, parallel-flow stability theory from incompressible to compressible flows, and with it came the result

† Email address for correspondence: a.tunney@auckland.ac.nz

that compressible flat-plate boundary layers were unstable to inviscid disturbances, whereas incompressible flows are stable in the inviscid limit. Mack (1984) performed extensive computations on the viscous and inviscid stability of various compressible boundary layers and revealed the existence of multiple 'Mack modes' of instability. This work particularly highlighted the importance of the generalised inflection point that arises in the compressible boundary layer, playing a role analogous to the classical inflection point of inviscid incompressible stability theory (for a detailed discussion see Schmid & Henningson 2001).

The effect of heat transfer on the stability of compressible boundary layers has been covered extensively in the case when the surface temperature is reduced. In this case a second generalised inflection point appears which, at a suitably high level of wall cooling, interacts with the first-mode instabilities (which arise as a consequence of the first generalised inflection point) so as to cancel their effect. At such a level of cooling, the first-mode instability is completely stabilised. Higher modes do however persist and cannot be eliminated by the introduction of wall cooling (Lees & Lin 1946; Mack 1975; Malik 1990*b*; Masad, Nayfeh & Al-Maaitah 1992). Transition control strategies, aimed at suppressing the instabilities, are based around the application of wall cooling and are therefore not practical, resulting in the exploration of other methods of active and passive control (see Fedorov 2011, and references contained therein).

When the heat transfer is from the surface to the fluid (i.e. the surface is heated) a different physical scenario arises. In the case of an incompressible fluid, such a scenario serves to modify the fluid density, which in turn induces a buoyancy force, thus serving to couple the momentum and energy transport. In this case, the streamwise velocity can develop so-called 'super-velocities'; the streamwise velocity field then attains values greater than the free-stream velocity. This 'overshooting' of the free-stream value by the streamwise velocity component is a direct consequence of the enhanced acceleration of the fluid due to the effect of thermal buoyancy, manifesting in a temperature induced pressure (the 'buoyancy' force). The nature of the spatially developing boundary layer ensures that this temperature induced pressure is a function of both the streamwise and normal coordinates, and hence the temperature, and thus the normal pressure gradient is also a function of both variables. As such, an additional streamwise pressure gradient appears in the horizontal momentum equation. Sufficiently far from the heated surface, the retarding effect on the fluid by the skin friction will be insufficient to counterbalance the enhanced acceleration of the flow due to the additional pressure component felt near the heated surface, and so the velocity 'overshoots' its free-stream value (see Denier & Mureithi 1996; Mureithi, Denier & Stott 1997, for further details).

The situation in a compressible boundary layer is similar. In this case, the overshoot results from the combined effect of a favourable pressure gradient and wall heating. Physically, the favourable pressure gradient acts across the entire boundary layer and accelerates the fluid. Heating the wall serves to reduce the fluid density and so enhances the effect of the pressure gradient on the fluid's acceleration, leading to a region in the flow in which the streamwise velocity overshoots its free stream value (a detailed discussion of this point can be found in Stewartson 1964). The existence of such flows, in the context of the existence of solutions of the compressible boundary-layer equations, has been demonstrated by McLeod & Serrin (1968*a*). A similar overshoot phenomena can arise in compressible flow over heated yawed cylinders (Reshotko & Beckwith 1957) and in three-dimensional flows with swirl (Back 1969).

The effect of surface heating in hypersonic flows is readily seen in the results of the HYTHIRM project, in which infrared imaging of the surface temperature of the US

Space Shuttle's was conducted during re-entry, at speeds above Mach 8 (see Gibson *et al.* 2010; Zamelda *et al.* 2010). Although the main focus of these experiments was to explore the efficacy of thermal imaging in measuring surface temperatures, they also allowed for the clear identification of regions of turbulent flow, in particular, they identified transition due to a protuberance on the shuttle surface (a 'speed hump' in the terminology of Gibson *et al.* 2010). Particularly intriguing is the presence of a wedge shape region of turbulent flow downstream of the nose of Shuttle Discovery (given the designation STS-119 in Gibson *et al.* 2010). Gibson *et al.* (2010), figure 8, denotes this region as 'turbulent flow of unknown origin'. Interestingly, this region exists downstream of the shuttle nose, where the surface temperature is markedly increased (see figure 11 of Gibson *et al.* 2010). This region of turbulent flow, clear in the Mach 8.43 re-entry images, is not evident in the higher Mach number re-entry images (designated STS-125 and STS-128, at Mach 14.33 and 14.73, respectively) shown in Gibson *et al.* (2010). This suggests that an instability mechanism is in operation, of unknown origin but perhaps triggered by the surface heating of the shuttle nose, and that this instability mechanism is sensitively dependent upon the flow Mach number.

There has long been a realisation that surface heating may play an important role in the overall flow dynamics of re-entry vehicles. This issue first seems to have been emphasised by Hirschel (1993) who noted the difference between terrestrial based experiments, which are often conducted in 'cold' facilities, where surface heating is not present, and real flight experiments (such as the shuttle re-entry experiments referred to earlier). This realisation has led to the development of new methods for prescribing non-uniform wall temperatures on models within wind tunnels (see for example Neely, Dasgupta & Choudhury 2014). With these developments, we can anticipate increased research into the effect of wall heating on the transition process in compressible (and in particular hypersonic) boundary layers.

Although the instability of buoyant boundary layers (the so-called mixed, free-forced convection boundary layers) has received considerable attention (Steinrück 1994; Denier & Mureithi 1996; Mureithi *et al.* 1997; Denier, Duck & Li 2005), we are not aware of any similar work on the impact of heat transfer (from the wall to the fluid) on the stability of a compressible boundary layer. The aforementioned incompressible theory demonstrates a rich and varied impact on the stability of the mixed, free-forced convection flows, in particular, issues surrounding non-uniqueness (Steinrück 1994), linear and fully nonlinear short waves confined to a degenerate critical layer at the position of maximum velocity (Denier & Mureithi 1996; Mureithi *et al.* 1997) and algebraically growing instabilities (Denier *et al.* 2005). This richness provides some tantalising hints as to the effect such heat transfer may have on compressible accelerating boundary layers. It is this problem we consider here, focussing on the inviscid instability and how the classical modes of Lees & Lin (1946) and Mack (1975, 1984) are modified through the development of a region of overshoot. We show that this affect is appreciable, with the most dramatic change being the development of a new family of unstable modes whose existence can be directly linked back to the presence of a maximum in the basic streamwise velocity.

2. Formulation

We consider the uniform flow of a viscous compressible fluid flowing over a heated rigid surface. We non-dimensionalise all length scales with respect to some characteristic length L, and velocity scales with respect to free-stream velocity U_∞,

leading to the usual non-dimensional parameters Re, the flow Reynolds number and $M = U_\infty/a_\infty$, the flow Mach number; here a_∞ is the speed of sound in the fluid. In the limit of large Reynolds number, the Navier–Stokes and enthalpy equations can be reduced in the usual way to the boundary-layer equations (see Malik 1990*a*). Generally, these require a numerical solution but some progress can be made if we appeal to a similarity solution in which the streamwise velocity u develops in a self-similar fashion. In this case the boundary-layer equations can be reduced to

$$(c_c f'')' + f f'' + \beta(1+k)(g - f'^2) = 0, \tag{2.1a}$$

$$(a_1 g' + a_2 f' f'')' + f g' = 0, \tag{2.1b}$$

where

$$\tau = (1+k)g - k f'^2, \quad c_c = \frac{\mu}{\tau}, \quad a_1 = \frac{c_c}{Pr}, \quad a_2 = \frac{2k}{1+k}\left(1 - \frac{1}{Pr}\right) c_c, \quad k = \frac{(\gamma-1)}{2} M^2; \tag{2.2a–e}$$

f', g, τ and μ are the streamwise velocity, enthalpy, temperature and fluid viscosity, non-dimensionalised by their values at the edge of the boundary layer, β is the Falkner–Skan pressure gradient parameter, γ is the heat capacity ratio, c_c is the Chapman-law viscosity–temperature coefficient and Pr is the (constant) Prandtl number. Primes denote differentiation with respect to the Mangler–Levy–Lees η coordinate, where

$$\mathrm{d}\eta \propto \frac{\mathrm{d}y}{\tau}, \tag{2.3}$$

with y being the coordinate normal to the plate. In deriving (2.1) we have assumed that the fluid obeys the ideal gas law, which taken together with the fact that the pressure does not vary across the boundary layer, yields $\rho\tau = 1$. In what follows we will employ a Chapman law for the variation of the temperature with viscosity, in which case $\mu = \tau$, allowing us to set $c_c \equiv 1$ in (2.1). This choice does not impact significantly upon the qualitative behaviour of the flow, but serves to considerably simplify the governing equations, thus facilitating our computations and the asymptotic analysis which we present in subsequent sections. The work presented here is intended to establish the fundamental stability behaviour of boundary layers with velocity overshoot prior to a more detailed analysis with sophisticated fluid models.

The boundary-layer equations (2.1) are solved subject to the boundary conditions

$$f(0) = f'(0) = 0, \quad g(0) = g_w, \quad f'(\eta), g(\eta) \to 1 \quad \text{as } \eta \to \infty, \tag{2.4a–c}$$

where g_w is the prescribed wall enthalpy. The equations are readily solved using standard quadrature techniques, allowing the effects of wall enthalpy, Mach number and other system parameters on the flow to be investigated. Solutions to these equations were first presented by Brown & Donoughe (1951). We present typical results, for the choice of $M = 6$, a wall enthalpy $g_w = 1.5$ and a Prandtl number $Pr = 0.72$ in figure 1. Figure 1(*a*), showing the streamwise velocity $f'(\eta)$, demonstrates the development of the region of velocity overshoot. This occurs for flows with a favourable pressure gradient ($\beta > 0$). As this favourable pressure gradient increases, the maximum of the streamwise velocity also increases and consequently the extent of the region of overshoot. Increases in the Mach number or wall enthalpy (not shown here) also serve to increase the velocity maximum, the extent of the region of overshoot and the boundary-layer thickness. This change in the behaviour of the

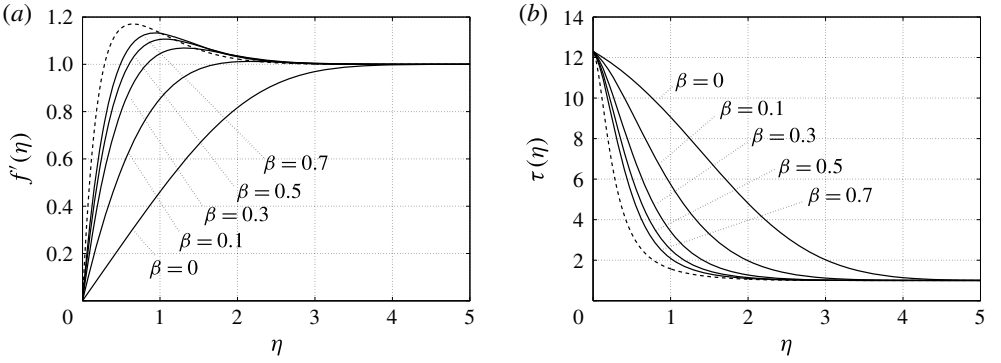

FIGURE 1. Plots of the streamwise velocity (a) and temperature (b) within the boundary layer for the case $M = 6$, $g_w = 1.5$ and $Pr = 0.72$. The dashed curve depicts the $\beta = 0.7$ case with the Sutherland law.

streamwise velocity profile has been well documented (see for example the discussions and results presented in Brown & Donoughe 1951; Cohen & Reshotko 1955; Li & Nagamatsu 1955; Reshotko & Beckwith 1957; Stewartson 1964; McLeod & Serrin 1968*a*,*b*; Bae & Emanuel 1997).

We emphasise that the overshoot is a physical manifestation of the change in the fluid density due to the wall heating, and not the particular viscosity–temperature law chosen. A qualitatively similar behaviour is observed if ones uses a nonlinear temperature viscosity law. The dashed curves in figure 1 illustrate that velocity overshoot is still a feature when using Sutherland's law, emphasising the fact that the changes between the Chapman and Sutherland profile are quantitative; the value of the maximum velocity is changed, increasing slightly for the Sutherland law model, and the position at which this maximum occurs changes, decreasing for the Sutherland fluid. From the perspective of the current work, the most significant difference in the predicted behaviour of the boundary layer for the Chapman versus Sutherland law's occurs in the very high Mach number limit. In that regime, the Sutherland law predicts an $O(1)$-thick temperature adjustment layer, whereas in the case of the Chapman law, this layer is logarithmically thin (and in both cases this layer occurs at the edge of the boundary layer); for a detailed discussion of this, see for example Fu, Hall & Blackaby (1993) and references contained therein. We can therefore be confident that a change in temperature viscosity law does not impact upon the fundamental physics driving the velocity overshoot as this occurs near the surface.

3. Linear stability analysis

We now turn our attention to the question of how, if at all, this region of overshoot affects the stability characteristics of the flow. To proceed we consider a small amplitude disturbance to the basic boundary-layer flow. A typical flow decomposition takes the form

$$p = \bar{p}(y) + \hat{p}(y)\exp\left[\mathrm{i}(\alpha x - \omega t)\right], \tag{3.1}$$

where $\bar{p}$ is the unperturbed flow (in this case the pressure), $\hat{p}$ the perturbation amplitude, α is the streamwise wavenumber of the disturbance and $\omega = \alpha c$, where c is the complex wavespeed (to be determined). Here, we focus on inviscid perturbations to the basic flow. Substituting these expansions into the full Navier–Stokes equations,

linearizing about the basic flow (and appealing to a parallel flow approximation, which is valid in this case as the inviscid instabilities have short wavelengths when compared to the developmental length scale of the boundary layer) we obtain the coupled system

$$D\hat{v} = \frac{D\bar{u}}{\bar{u}-c}\hat{v} + \frac{\mathrm{i}\alpha(\bar{T}-M^2(\bar{u}-c)^2)}{\gamma M^2(\bar{u}-c)}\hat{p}, \tag{3.2a}$$

$$D\hat{p} = -\frac{\mathrm{i}\alpha\gamma M^2(\bar{u}-c)}{\bar{T}}\hat{v}, \tag{3.2b}$$

where $\hat{v}$ and $\hat{p}$ are the normal velocity and pressure perturbation amplitudes, $\bar{u}$ and $\bar{T}$ are the boundary-layer velocity and temperature (i.e. frozen at a particular streamwise location and so that all are treated as functions of y only) and $D \equiv \mathrm{d}/\mathrm{d}y$. These must be solved subject to the usual inviscid boundary conditions of no penetration at the surface and the constraint that the disturbance is confined to the boundary layer

$$\hat{v}(0) = 0, \quad \hat{v} \text{ bounded as } y \to \infty. \tag{3.3}$$

We focus on the temporal stability problem and so consider real values of α with the complex eigenvalues c, with $\mathrm{Im}(c) > 0$ representing temporal growth, to be determined.

Cross-differentiation of these equations allows us to write the system as a single second-order equation for the pressure perturbation amplitude

$$D^2\hat{p} - \left(\frac{2D\bar{u}}{\bar{u}-c} - \frac{D\bar{T}}{\bar{T}}\right)D\hat{p} - \alpha^2\left(1 - \frac{M^2(\bar{u}-c)^2}{\bar{T}}\right)\hat{p} = 0 \tag{3.4}$$

with boundary conditions

$$D\hat{p}(0) = 0, \quad \hat{p} \text{ bounded as } y \to \infty. \tag{3.5}$$

Alternatively we can derive a single equation for the normal velocity perturbation amplitude as

$$D\left\{\frac{(\bar{u}-c)D\hat{v} - (D\bar{u})\hat{v}}{\bar{T} - M^2(\bar{u}-c)^2}\right\} = \alpha^2\frac{\bar{u}-c}{\bar{T}}\hat{v}, \tag{3.6}$$

to be solved subject to boundary conditions (3.3). These forms prove useful for our subsequent asymptotic analysis. We will refer to either of these equations as the (compressible) Rayleigh equation.

Before proceeding with a description of the major features of the eigenspectrum of this system, we first note that the inviscid equations are singular at points where $\bar{u} = c$, thus making the numerical determination of the structure of inviscid neutral modes (i.e. those with $\mathrm{Im}(c) = 0$) difficult. We also note that the eigensolutions of the compressible Rayleigh equation occur in complex conjugate pairs; if c is an eigenvalue with $\hat{v}$ the corresponding eigenfunction, then the complex conjugate of c is also an eigenvalue (with corresponding eigenfunction the complex conjugate of $\hat{v}$).

3.1. *Local analysis of the singular point at* $\bar{u} = c$

As noted above, the Rayleigh equation is singular at the point $y = y_c$ where $\bar{u} = c_r$, and c_r is the real part of the neutral (i.e. $c_i = 0$) eigenvalue. In order to explore the critical layer structure of the neutral eigenmodes, we consider two cases, namely when the critical layer is not located at the position of the velocity maximum and the case when it occurs precisely at the location of the velocity maximum.

3.1.1. *Case 1:* $c \neq \bar{u}_{max}$

In order to develop a solution, we first note that since $Y \equiv y - y_c = 0$ is a regular singular point of equation (3.6) we seek an expansion for $\hat{v}$ about $Y = 0$ in the form

$$\hat{v} = a_0 Y^n + a_1 Y^{n+1} + \cdots . \tag{3.7}$$

Substitution of this expansion into (3.6) yields, at leading order in powers of Y, the indicial equation

$$\bar{T}_c D\bar{u}_c n(n-1)a_0 = 0; \tag{3.8}$$

here a subscript c denotes a quantity evaluated at the critical point. As $\bar{T} > 0$ everywhere and $D\bar{u}_c \neq 0$, the choice $n = 1$ yields a solution in the form of a regular series expansion in powers of Y:

$$\hat{v}_A = a_0 Y + a_1 Y^2 + a_2 Y^3 + \cdots \tag{3.9}$$

where the first two coefficients are given by

$$a_1 = \frac{1}{2}\left(\frac{D^2\bar{u}_c}{D\bar{u}_c}\right) a_0, \quad a_2 = \frac{1}{6}\left(\alpha^2 + \frac{D^3\bar{u}_c}{D\bar{u}_c}\right) a_0. \tag{3.10a,b}$$

Standard theory on the local solution of ordinary differential equations then guarantees that there is a second linearly independent solution on the form

$$\hat{v}_B = \hat{v}_A \log Y + b_0 + b_1 Y + b_2 Y^2 + \cdots . \tag{3.11}$$

Substituting this expression into (3.6) we find that a_0 and b_0 are related via the expression

$$a_0 = b_0 \frac{\bar{T}_c}{D\bar{u}_c}\left[D\left(\frac{D\bar{u}}{\bar{T}}\right)\right]_c . \tag{3.12}$$

This expansion can be carried to higher order, allowing us to determine b_2, b_3 etc in terms of the leading-order terms b_0 and b_1. For the sake of brevity, we do not include these expressions here. We note however, that if the condition

$$\left[D\left(\frac{D\bar{u}}{\bar{T}}\right)\right]_c = 0, \tag{3.13}$$

is satisfied, then from (3.12), $a_0 = 0$ and so $a_i \equiv 0$, for all $i \geqslant 1$ and the logarithmic singularity in the second linearly dependent solution (3.11) is removed. This condition, when satisfied, also ensures that the Reynolds stress is continuous across the critical layer. The presence of such a generalised inflection point is a sufficient condition for the existence of a neutral, subsonic, inviscid disturbance with wavenumber $\alpha = \alpha_{sn} > 0$, and that this is adjacent to unstable eigenvalues at $\alpha < \alpha_{sn}$ using the notation of Mack (1987) for neutral wavenumbers.

3.1.2. *Case 2:* $c = \bar{u}_{max}$

Suppose that the neutral mode is such that $c = \bar{u}_{max}$. Since the streamwise velocity has a maximum at this point, $D\bar{u}_c = 0$ and the point $Y = 0$ is still a regular singular point. With the expansion for $\hat{v}$ as before, we find the indicial equation is now given by

$$D^2\bar{u}_c\bar{T}_c^2(n+1)(n-2)\hat{a}_0 = 0, \tag{3.14}$$

with two possible solutions $n = -1$ and $n = 2$ (noting that $D^2\bar{u}_c \neq 0$).

The $n = 2$ case yields the solution

$$\hat{v}_A = \hat{a}_0 Y^2 + \hat{a}_1 Y^3 + \cdots \tag{3.15}$$

where

$$\hat{a}_1 = \frac{1}{3}\left(\frac{D^3\bar{u}_c}{D^2\bar{u}_c}\right)\hat{a}_0 \tag{3.16}$$

$$\hat{a}_2 = \left(\frac{1}{10}\alpha^2 + \frac{1}{12}\frac{D^4\bar{u}_c}{D^2\bar{u}_c}\right)\hat{a}_0. \tag{3.17}$$

A second linearly independent solution can be written as

$$\hat{v}_B = \hat{v}_A \log Y + \hat{b}_0 Y^{-1} + \hat{b}_1 + \hat{b}_2 Y + \cdots \tag{3.18}$$

which when substituted into the compressible Rayleigh equation yields, upon equating orders of Y,

$$\hat{a}_0 = \hat{b}_0\left[-\frac{1}{2}\alpha^2 + \frac{3}{2}\frac{D^2\bar{T}_c}{\bar{T}_c} - \frac{3}{2}\frac{D^3\bar{u}_c D\bar{T}_c}{D^2\bar{u}_c\bar{T}_c} - \frac{5}{12}\frac{D^4\bar{u}_c}{D^2\bar{u}_c} + \frac{2}{3}\frac{(D^3\bar{u}_c)^2}{(D^2\bar{u}_c)^2}\right]. \tag{3.19}$$

The difference between this case and the previous generalised inflection point case is now evident. In order to remove the logarithmic term, the term in the brackets in (3.19) must necessarily be zero, thus serving to (possibly) determine the neutral wavenumber α_c. However, in this case, the second linearly independent solution, given by (3.18), still possesses an algebraic singularity.

In figure 2 we present plots of the location (scaled by δ^*, the boundary-layer displacement thickness) of the generalised points of inflection, and the corresponding values of the velocity at those points, for a boundary layer with $g_w = 1.5$ as a function of the pressure-gradient parameter β. We observe that for any flow with $\beta > 0$ (i.e. all those exhibiting a velocity overshoot), there are two generalised points of inflection (the solid lines in figure 2) as opposed to just one when $\beta = 0$. The lower of these (on both plots) is positioned below the velocity maximum and moves closer to the wall with increasing β, ultimately moving into the overshoot region when $\beta \approx 0.55$. The second generalised inflection point enters the boundary layer from far field (i.e the free stream where $\bar{u} = 1$) at $\beta = 0$, and remains on the free-stream side of the velocity maximum as β increases. The existence, and location, of the generalised points of inflection have important consequences for the spectrum of unstable eigenmodes of the compressible Rayleigh equation.

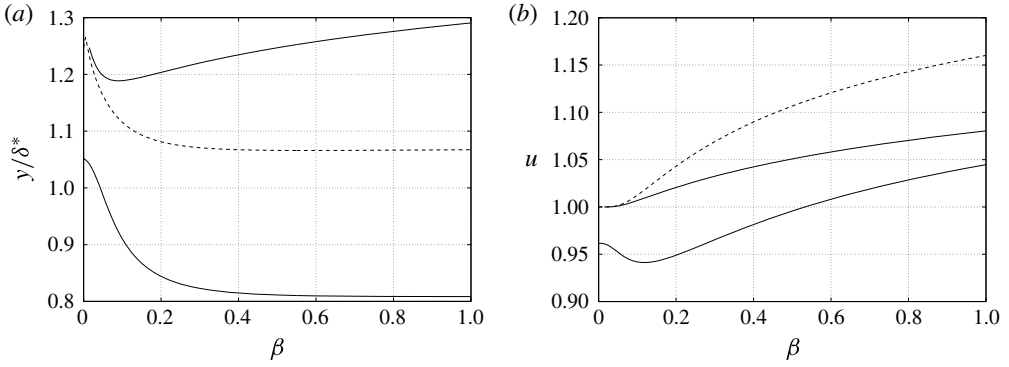

FIGURE 2. Plots of (*a*) the position of the points of generalised inflection points (solid) and the maximum velocity (dashed) and (*b*) the corresponding values of the velocity at this location versus the pressure-gradient parameter β. Results are for the case of a heated-wall ($g_w = 1.5$) compressible ($M = 6$) boundary layer with $Pr = 0.72$.

4. The inviscid instability

In order to solve the inviscid stability problem defined by (3.6), we chose an iterative scheme. This choice is motivated by both ease of implementation and its ability to be coupled to the boundary-layer solver, thus allowing rapid and easy continuation of solutions with respect to the various system parameters (in particular β and M). Thus a classical shooting method, based upon the iterative update of the eigenvalues using the boundary condition at the wall as the target converged solution, is used. The scheme uses a fourth-order Runge–Kutta scheme to integrate from the free stream, chosen at some suitably large value of y, to the wall at $y = 0$. To set up the iterative scheme, we make use of the far-field form of the disturbances, which can be obtained by substituting the free-stream boundary conditions into (3.4) and (3.2*b*), to give

$$\left.\begin{aligned} \hat{p} &\sim \exp(-\alpha y\sqrt{1 - M^2(1-c)^2}) \\ \hat{v} &\sim \frac{-\mathrm{i}\sqrt{1 - M^2(1-c)^2}}{\gamma M^2(1-c)}\hat{p} \end{aligned}\right\} \quad \text{as } y \to \infty. \tag{4.1}$$

These limiting values are used as initial conditions for integration from a sufficiently large value of y (at least ten times the boundary-layer thickness). For all computational results reported here, a variable spaced grid was used, with clustering of grid points around the wall, and near any other areas of rapid variation (critical layers for example). The average step size for the grid was 0.01. Newton–Raphson was implemented for the local eigenvalue search with an error tolerance on the desired boundary condition of $O(10^{-10})$. Extensive testing of convergence was undertaken in arriving at these values.

Our results are presented in figures 3–6 for a variety of values of the pressure-gradient parameter β (but with identical values of the Mach number and wall enthalpy). Consider first figure 3, where we plot the values of Im(c) and wavespeed Re(c) versus disturbance wavenumber. Here we observe three distinct families of eigenvalues (a continuous set of eigenvalues), each containing one or more amplified modes (local maxima on the Im(c) plot) of disturbance. Two of these correspond to

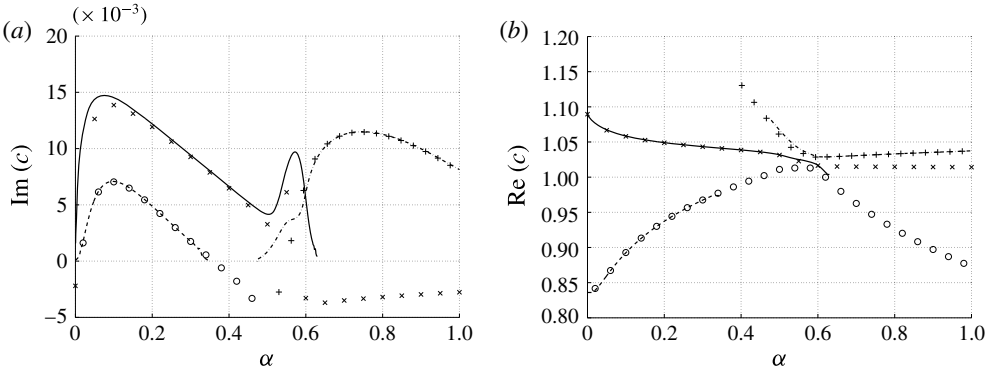

FIGURE 3. Upstream family (dashed), first downstream family (dotted) and new family (solid) of inviscid eigenvalues and corresponding viscous eigenvalues (○, +, ×) for a representative overshoot boundary layer with $M = 6$, $g_w = 1.5$, $\beta = 0.4$ and $Pr = 0.72$.

the classical inviscid instability of a compressible boundary layer; these have been labelled as upstream and downstream to conform to the convention set down by Mack (1987). We show only a portion of the wavenumber spectrum (up to $\alpha = 1$) as we are concerned mainly with the presence of the new eigenmode contained within a family of eigenvalues presented as a solid line in figure 3. This new instability exists along with the traditional first mode and higher modes of instability. For this value of β, the growth rate $\mathrm{Im}(\omega)$ of the new mode is comparable to the classical modes. The classical downstream family is however unstable for smaller disturbance wavelengths (i.e. higher disturbance wavenumber). Considering the corresponding wavespeed in figure 3(*b*), we observe that this new instability has a wavespeed greater than unity over the entire spectrum of unstable wavelengths, approaching unity as the neutral (i.e. critical) point is approached.

Figure 3, and subsequent figures, also show values of the eigenvalues obtained from the numerical solution of the full viscous linearized stability equations at high Reynolds number ($R = 10^5$ with $R \sim O(Re^{1/2})$. For details of the methodology see Malik 1990*a*). These results provide an excellent comparison with, and confirmation of, our inviscid results and also serve to demonstrate that the correct sign of $\mathrm{Im}(c)$ has been chosen for the inviscid eigenvalues. The lower $\mathrm{Im}(c)$ values of the high Reynolds number viscous results also confirm that the new mode of instability is inviscidly unstable.

Considering the results presented in figure 3 in more detail, we first make the observation that the unstable family represented by the dashed line corresponds to the upstream family, originating from the point $c = 1 - 1/M$ at $\alpha = 0$. This family contains only the traditional mode 1 disturbance and is unstable over a finite band of streamwise wavenumbers, becoming neutrally stable at a value of $c = c_r + \mathrm{i}0$ corresponding to the velocity at the lower of the two generalised inflection points (see figure 2*a*). The change in the spectrum of this mode with β can be seen from figures 3–5. As β increases, the maximum growth rate of this mode increases and the corresponding neutral wavenumber also increases, the neutral mode still being located at the critical layer position defined by the lower of the two generalised inflection points. A similar qualitative change in this first unstable mode is seen if we increase the flow Mach number (results not shown).

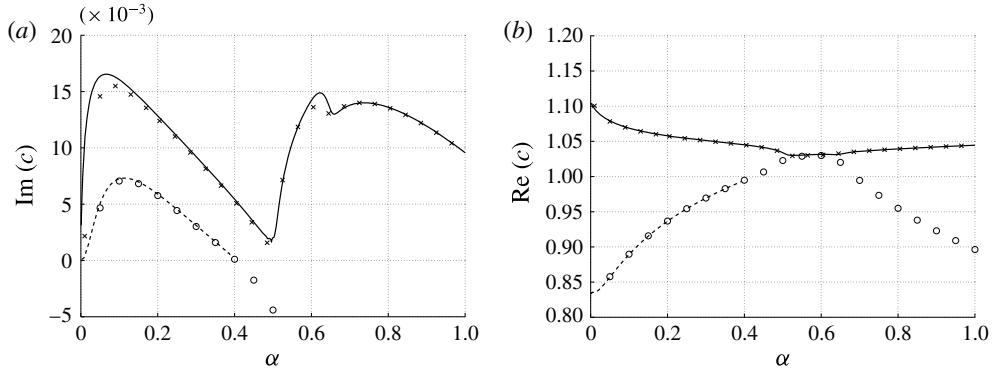

FIGURE 4. Upstream family (dashed), new family (solid) of inviscid eigenvalues and corresponding viscous eigenvalues (○, ×) for a representative overshoot boundary layer with $M = 6$, $g_w = 1.5$, $\beta = 0.5$ and $Pr = 0.72$.

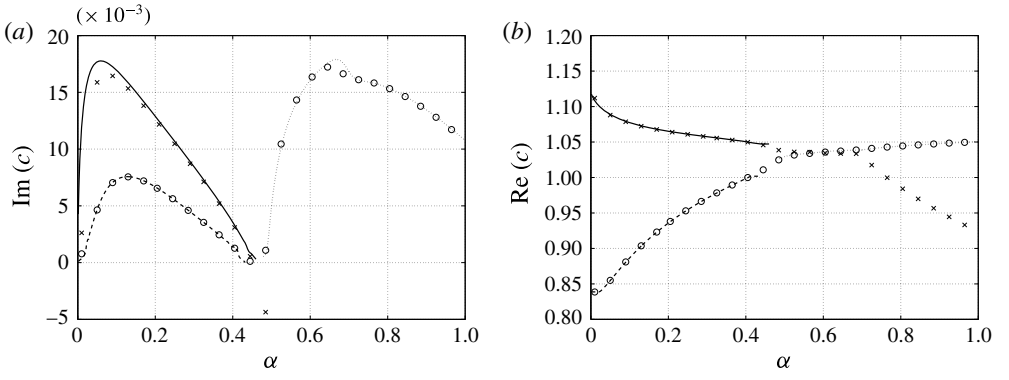

FIGURE 5. Upstream family (dashed), first downstream family (dotted) and new family (solid) of inviscid eigenvalues and corresponding viscous eigenvalues (○, +, ×) for a representative overshoot boundary layer with $M = 6$, $g_w = 1.5$, $\beta = 0.6$ and $Pr = 0.72$.

A second family of eigenvalues, represented by the dotted line in figure 3, corresponds to the first downstream family of Mack (1987). There are infinitely many downstream modes, of which only the first attains a significant growth rate. This family arises when $c = 1 + 1/M$ at a discrete sequence of wavenumbers α_{dn} (the first of which is $\alpha_{d1} = 0$) and remains neutral until c decreases below $\bar{u}_{max}$; for the case of $\beta = 0.4$ we find that $\bar{u}_{max} \approx 1.08$, agreeing with the numerical value of the neutral wavenumber.

Most significantly however is the new unstable mode present in figure 3, which is in a new family represented by the solid line. This new mode arises as a direct result of the velocity overshoot, as can be seen by noting that for small α, the wavespeed approaches $c = \bar{u}_{max}$ (which for $\beta = 0.4$ is approximately 1.09).

This family also exhibits a second local maximum in the growth rate. Using a simple continuation process in β we can demonstrate that this second maximum corresponds to the traditional Mack mode 2 disturbance. This mode 2 has critical wavespeed approaching 1 and becomes stable at a value of c that does not correspond to either of the generalised points of inflection, instead appearing to approach the

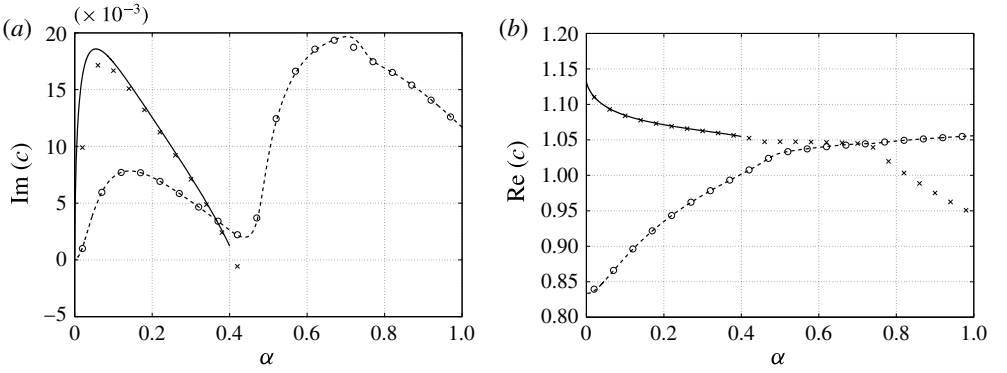

FIGURE 6. Upstream family (dashed), new family (solid) of inviscid eigenvalues and corresponding viscous eigenvalues (○, ×) for a representative overshoot boundary layer with $M = 6$, $g_w = 1.5$, $\beta = 0.7$ and $Pr = 0.72$.

limiting value of $c_r = 1$. What is also clear from figure 3 is that the eigenmodes interact, exchanging identity as the wavenumber α is varied; this is most readily seen in figure 3(*b*). The viscous and inviscid results deviate slightly indicating that this behaviour is sensitive to viscosity. This exchange of identity is explored in detail in Mack (1987). The relationship between the new family (the solid curve and crosses) and the upstream family (the dashed curve and open circles) becomes clearer when we observe their similar wavespeeds (for $\alpha > 0.6$) which then diverge for smaller α, the growth rates showing a similar trend, increasing with decreasing α.

This interaction, and relationship between the unstable modes presented here, hints at a complicated folding structure in the curves of neutral stability, something we explore in detail in work currently being prepared for publication. The relationship between the new mode and the 'classical' Mack modes is further complicated as we increase the pressure-gradient parameter β.

Figure 4 shows eigenvalues for the case of $\beta = 0.5$, where we see that the near-intersection of eigenvalues at $\alpha = 0.6$ for $\beta = 0.4$ observed in figure 3 has occurred by the time β has increased to 0.5. The two families have merged; the new family now contains the new mode and the traditional mode 2 and mode 3 disturbances. The upstream family (dashed curve) still has a finite band of instability corresponding to the traditional mode 1 disturbance, terminating at a value of c_r corresponding to the lower of the generalised inflection points.

This interaction of the different unstable modes becomes further complicated as we increase β yet again. In figure 5 we can see that, for $\beta = 0.6$, the mode 2 and 3 disturbances have disconnected from the new family and can now be classified in the first downstream family. The upstream modes (dashed curve) neutral point again corresponds to the lower most point of inflection. Comparison with the results of figure 2 suggests that the critical values for the new mode and the Mack downstream mode do not correspond to any distinguished point when referenced to the position of the (two) generalised inflection points or the position of maximum velocity.

By $\beta = 0.7$, shown in figure 6, the first-mode disturbance has grown significantly such that the upstream family has merged with the downstream family and it now contains the second and third-mode unstable regions. Changing the flow's Mach number serves to modify the growth rate of this new mode, as can be seen from the results for Mach numbers $M = 5$–7 which are presented in figure 7. Again, a

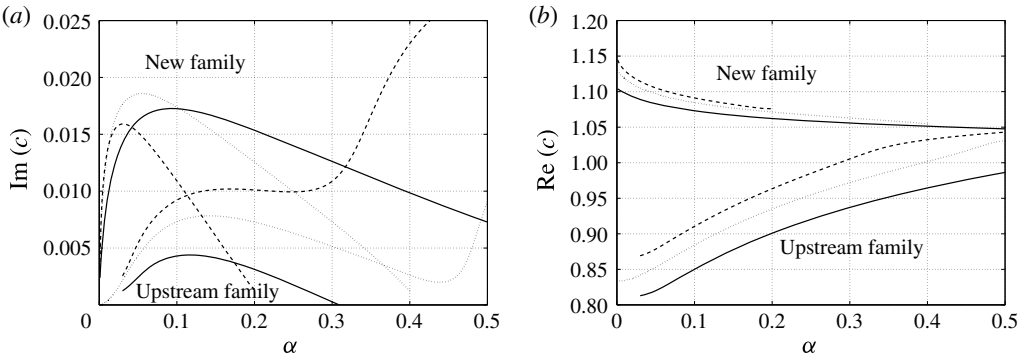

FIGURE 7. Inviscid eigenvalues for the case of $g_w = 1.5$, $\beta = 0.7$ and Mach numbers $M = 5$ (solid), $M = 6$ (dotted) and $M = 7$ (dashed).

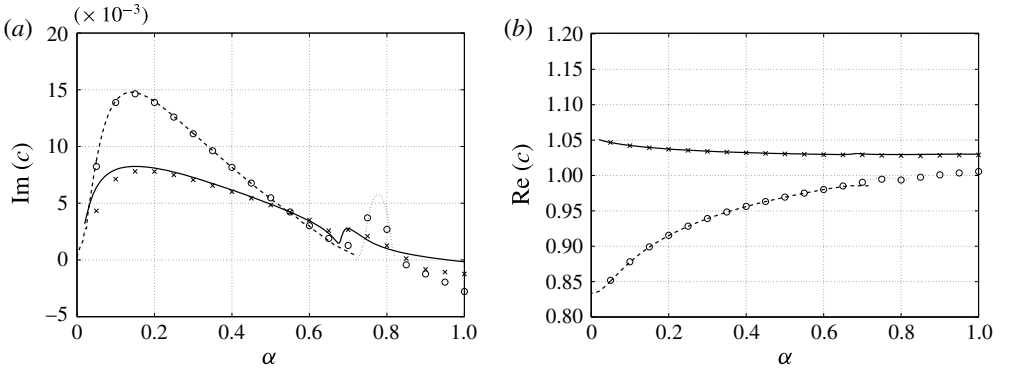

FIGURE 8. Upstream family (dashed), first downstream family (dotted) and new family (solid) of inviscid eigenvalues and corresponding viscous eigenvalues (○, ×) for a representative overshoot boundary layer with $M = 6$, $g_w = 1.5$, $\beta = 0.7$ and $Pr = 1$.

qualitatively similar behaviour is found at different Prandtl numbers; figure 8 shows results for $Pr = 1$, the new mode having similar growth rates to the classical upstream Mach mode. These results confirm that this new mode is generic in that it occurs in boundary-layer flows favourable pressure gradients and appreciable levels of heat transfer at the surface.

We conclude this section with the observation that the bracketed term in (3.19) does not provide any useful reference point with regards to the neutral (or critical) points observed in figures 4–6. Considering the particular case of $\beta = 0.7$, the bracketed part of (3.19) reduces to

$$-\tfrac{1}{2}\alpha^2 + 1.427 \tag{4.2}$$

which equals zero when $\alpha \approx 1.69$. This does not correspond to any of the neutral wavenumbers seen in figure 6; we note that the upstream family becomes damped around $\alpha = 1.31$.

In order to explore the structure of this new mode further, we now turn our attention to description of the small wavenumber (long wavelength) limit of (3.6).

5. The small wavenumber limit

Lees & Lin (1946) developed series solutions for (3.6), valid in the small wavenumber limit, in powers of α^2 of the form $\hat{v} = C_1\hat{v}_1 + C_2\hat{v}_2$, where $\hat{v}_1$ and $\hat{v}_2$ represent the two linearly independent solutions, given by

$$\hat{v}_1 = (\bar{u} - c)\left(I + \alpha^2 \int_0^y I\frac{(\bar{u} - c)^2}{\bar{T}}\,\mathrm{d}y^* + O(\alpha^4)\right), \tag{5.1}$$

$$\hat{v}_2 = (\bar{u} - c)\left(1 + \alpha^2 \int_0^y \frac{(\bar{u} - c)^2}{\bar{T}}\,\mathrm{d}y^* + O(\alpha^4)\right), \tag{5.2}$$

where

$$I = \int_0^y \left[\frac{\bar{T}}{(\bar{u} - c)^2} - M^2\right]\,\mathrm{d}y^*, \tag{5.3}$$

and C_1 and C_2 are arbitrary constants. Provided that $c \neq 0$, in the limit $\alpha \to 0$, C_2 must be zero in order to satisfy the wall boundary condition. In order to satisfy the boundedness condition, the integral I must approach a constant. Thus the integrand appearing in (5.3) must tend to zero as $y \to \infty$. Noting that both $\bar{T}$ and $\bar{u}$ tend to unity as $y \to \infty$, we must therefore have $M^2(1 - c)^2 = 1$. Hence the neutral wavespeed is given by

$$c = c_0 = 1 \pm \frac{1}{M}. \tag{5.4}$$

These neutral mode solutions are termed sonic modes, since in this case the disturbance travels downstream or upstream at the local speed of sound.

Our numerical solutions presented in the previous section demonstrate that there is another neutral mode present as $\alpha \to 0$, for which $c \to \bar{u}_{max}$. In general, $\bar{u}_{max} \neq 1 + 1/M$ so $\hat{v}_1$ will not necessarily be bounded, violating the free-stream boundary condition. This immediately suggests that each of the two linearly independent solutions will play a different role in different regions of the flow. The wall boundary condition forces us to choose the $\hat{v}_1$ solution whereas the boundedness conditions forces us to choose the $\hat{v}_2$ solution. Thus, in the small α limit, we expect a solution structure in which

$$\hat{v} \sim \begin{cases} \hat{v}_1 \sim (\bar{u} - c)I, & y < y_c, \\ V, & y \text{ near } y_c, \\ \hat{v}_2 \sim (\bar{u} - c), & y > y_c, \end{cases} \tag{5.5}$$

where y_c is the position of the velocity maximum. Our aim is therefore to provide an asymptotic description of the new unstable mode in the limit $\alpha \to 0$, effectively determining the function V in (5.5).

To investigate this behaviour for small α, we write $c = \bar{u}_{max} + \alpha^m c_1$, where c_1 may be complex, and introduce a new scaled coordinate $z = (y - y_c)/\delta$, where $\delta = \alpha^n$ and $n > 0$. Expanding all flow quantities in a Taylor series about $y = y_c$, (3.6) can be written as

$$\frac{\mathrm{d}}{\mathrm{d}z}\left\{\left[\frac{\frac{1}{2}\lambda z^2 + \frac{1}{6}D^3\bar{u}_c\alpha^n z^3 - \alpha^{m-2n}c_1 + O(\alpha^{2n})}{\bar{T}_c + D\bar{T}_c\alpha^n z + O(\alpha^{2n})}\right]\frac{\mathrm{d}\hat{v}}{\mathrm{d}z}\right.$$
$$\left. - \left[\frac{\lambda z + \frac{1}{2}D^3\bar{u}_c\alpha^n z^2 + O(\alpha^{2n})}{\bar{T}_c + D\bar{T}_c\alpha^n z + O(\alpha^{2n})}\right]\hat{v}\right\} = O(\alpha^{2+(2/n)}) \tag{5.6}$$

where a subscript c indicates a quantity evaluated at y_c; for convenience we have defined $\lambda = D^2\bar{u}_c$. A simple dominant balance argument serves to determine $m = 2n$. We note at this point our numerical results strongly suggest $m = 2/3$, and hence $n = 1/3$. However m, and hence n, must be determined *a posteori* by matching the solution across the various distinguished asymptotic layers that arise in the flow. We consider the solution in three regions defined as:

Region L: $0 < y \ll y_c$, in which the solution must satisfy the boundary condition $\hat{v}(0) = 0$,

Region I: $|y - y_c| \sim O(\delta)$, in which the solution must match with region L and region R which is defined as

Region R: $y_c < y \sim O(1)$, in which the solution must satisfy the far-field boundary condition (4.1).

5.1. *The leading order, $O(\alpha^0)$, solution*

Region L

In this region we define $\hat{v} = \hat{v}_L$ and note that the boundary condition to be satisfied is $\hat{v}_L(0) = 0$. In this region, the stability equation (3.6) can be written as

$$D\left\{\frac{(\bar{u} - \bar{u}_{max} - \delta^2 c_1)D\hat{v}_L - (D\bar{u})\hat{v}_L}{\bar{T} - M^2(\bar{u} - \bar{u}_{max} - \delta^2 c_1)^2}\right\} = \frac{\bar{u} - \bar{u}_{max} - \delta^2 c_1}{\bar{T}}\delta^6\hat{v}_L. \tag{5.7}$$

We define

$$\hat{v}_L = \delta^L(v_{L0} + \cdots), \tag{5.8}$$

where the amplitude δ^L will be determined relative to the amplitude in the regions I and R. At leading order in powers of δ, (5.7) has the general solution

$$v_{L0} = A_1(\bar{u} - \bar{u}_{max})I_L + A_2(\bar{u} - \bar{u}_{max}), \tag{5.9}$$

where

$$I_L = \int_0^y \left[\frac{\bar{T}}{(\bar{u} - \bar{u}_{max})^2} - M^2\right] \mathrm{d}y, \tag{5.10}$$

and A_1 and A_2 are constants of integration. In order to satisfy the wall boundary condition $\hat{v}_L(0) = 0$, A_2 must be zero as $\bar{u} - \bar{u}_{max} \neq 0$ at $y = 0$. Taking the limit $y \to y_c^-$ we have

$$\hat{v}_L = \delta^L A_1\left[-\frac{2\bar{T}_c}{3\lambda}(y - y_c)^{-1} + \left(\frac{4}{9}\frac{D^3\bar{u}_c\bar{T}_c}{\lambda^2} - \frac{D\bar{T}_c}{\lambda}\right) + O(y - y_c)\right] + \cdots. \tag{5.11}$$

This is now in a suitable form to match with the solution in Region I.

Region I

In this region $|y - y_c| \sim O(\delta)$. Defining $z = (y - y_c)/\delta$ and setting $\hat{v} = \hat{v}_I$ where

$$\hat{v}_I = \delta^I(v_{I0} + \cdots), \tag{5.12}$$

equation (5.6) yields, at leading order,

$$\frac{\mathrm{d}}{\mathrm{d}z}\left\{\left(\frac{1}{2}\lambda z^2 - c_1\right)\frac{\mathrm{d}v_{I0}}{\mathrm{d}z} - \lambda z v_{I0}\right\} \equiv \mathscr{L}_I v_{I0} = 0, \tag{5.13}$$

where we have introduced the differential operator $\mathscr{L}_I$ for later reference. The general solution for v_{I0} is given by

$$v_{I0} = B_1 \left[(z^2 + \Gamma) \arctan\left(\frac{z}{\sqrt{\Gamma}} \right) + z\sqrt{\Gamma} \right] + B_2[z^2 + \Gamma], \tag{5.14}$$

where $\Gamma = -2c_1/\lambda$. To match with the solution (5.11) in region L we consider the limiting form of (5.14) as $z \to -\infty$,

$$v_{I0} \sim \left[-\frac{\pi}{2} B_1 + B_2 \right] z^2 + \left[-\frac{\pi}{2} \Gamma B_1 + \Gamma B_2 \right] + \left[-B_1 \frac{2\Gamma^{3/2}}{3} \right] z^{-1} + \cdots . \tag{5.15}$$

By setting

$$B_2 = \frac{\pi}{2} B_1 \tag{5.16}$$

the z^2 and constant terms in (5.15) are identically zero, thus allowing us to match with the leading-order behaviour of v_{L0}. This yields

$$\delta^L A_1 \left(-\frac{2\bar{T}_c}{3\lambda} \right) = \delta^{I+1} B_1 \left(-\frac{2\Gamma^{3/2}}{3} \right), \tag{5.17}$$

serving to determine the relative amplitude of the normal velocity in the two layers, and relating A_1 and B_1 via

$$B_1 = \frac{\bar{T}_c}{\lambda \Gamma^{3/2}} A_1. \tag{5.18}$$

With this expression, we then have, in the limit $z \to \infty$,

$$v_{I0} = \frac{A_1 \pi \bar{T}_c}{\lambda \Gamma^{3/2}} z^2 + \frac{A_1 \pi \bar{T}_c}{\lambda \Gamma^{1/2}} - \frac{2A_1 \bar{T}_c}{3\lambda} z^{-1} + \cdots , \tag{5.19}$$

which will be used to match the solution in region R.

Region R

In a similar fashion to the analysis of region L, we set $v_R = \delta^R v_{R0}$, and at leading order obtain a general solution of (5.7) in the form

$$v_{R0} = C_1(\bar{u} - \bar{u}_{max}) I_R + C_2(\bar{u} - \bar{u}_{max}), \tag{5.20}$$

where I_R denotes the integral

$$I_R = \int_y^\infty \left[\frac{\bar{T}}{(\bar{u} - \bar{u}_{max})^2} - M^2 \right] \mathrm{d}y. \tag{5.21}$$

The leading-term expansion of v_{R0} as $y \to y_c^+$ must match the leading term in the v_{I0} expansion as $z \to +\infty$. Noting that $(\bar{u} - \bar{u}_{max}) I_R \sim O((y - y_c)^{-1})$ as $y \to y_c^+$, we must therefore choose C_1 to be zero. Thus the leading-order behaviour of $\hat{v}_R$ as $y \to y_c^+$ is therefore

$$\hat{v}_R = \tfrac{1}{2} \delta^R C_2 \lambda (y - y_c)^2 + \cdots , \tag{5.22}$$

which will match with (5.19) if $\hat{v}_R \sim O(\delta^{I-2})$ (i.e. $\mathrm{R} = \mathrm{I} - 2$) and we choose

$$C_2 = \frac{2\pi \bar{T}_c}{\lambda^2 \Gamma^{3/2}} A_1. \tag{5.23}$$

From (5.20) we then have

$$\hat{v}_R \sim \delta^R C_2 (1 - \bar{u}_{max}) + \cdots \quad \text{as } y \to \infty, \tag{5.24}$$

where we have used the fact that $\bar{u} \to 1$ as $y \to \infty$.

To close the problem, we now turn our attention to the far-field boundary condition (4.1). In order to consider this far-field region, we define a new stretched coordinate $\bar{y} = \delta^3 y$; at this scale, the right-hand side of (3.6) enters at leading order. Taking the free-stream values of the streamwise velocity and temperature, (4.1) reduces to

$$\frac{\mathrm{d}^2 \hat{v}_F}{\mathrm{d}\bar{y}^2} = (1 - M^2 (1 - \bar{u}_{max})^2) \hat{v}_F, \tag{5.25}$$

which has a bounded solution given by

$$\hat{v}_F = F \exp(-\Omega \bar{y}), \tag{5.26}$$

where we have defined $\Omega^2 = 1 - M^2 (1 - \bar{u}_{max})^2$. In the limit $\bar{y} \to 0$ we have

$$\hat{v}_F \to F \left(1 - \Omega \bar{y} + \frac{\Omega^2}{2} \bar{y}^2 + \cdots \right), \tag{5.27}$$

and the solution will match with region R if

$$F = C_2 (1 - \bar{u}_{max}) \equiv A_1 \frac{2\pi \bar{T}_c}{\lambda^2 \Gamma^{3/2}} (1 - \bar{u}_{max}). \tag{5.28}$$

This constitutes an entire solution for $\hat{v}_F$. Since the equation for $\hat{v}$ is linear we can, without loss of generality, take $\hat{v}_F = O(1)$, this then serves to determine the relative magnitudes of the disturbance velocity in regions L, I and R. Hence $\hat{v}_R \sim O(1)$, $\hat{v}_I \sim O(\delta^2)$ and $\hat{v}_L \sim O(\delta^3)$.

To summarise, we have obtained the leading-order approximation for $\hat{v}$ in all regions:

$$\hat{v} \approx A_1 \begin{cases} \delta^3 (\bar{u} - \bar{u}_{max}) I_L & \text{for } 0 < y < y_c, \\ \delta^2 \dfrac{\bar{T}_c}{\lambda \Gamma^{3/2}} \left[(z^2 + \Gamma) \left(\arctan \dfrac{z}{\sqrt{\Gamma}} + \dfrac{\pi}{2} \right) + z\sqrt{\Gamma} \right] & \text{for } |y - y_c| \sim O(\delta), \\ \dfrac{2\pi \bar{T}_c}{\lambda^2 \Gamma^{3/2}} (\bar{u} - \bar{u}_{max}) & \text{for } y > y_c. \end{cases} \tag{5.29}$$

At this stage of the analysis, c_1 and n are not formally determined, in order to do so, the asymptotic expansions must be taken to higher order. Some of this analysis is presented in appendix A. Important however is the fact that the leading-order analysis of the small wavenumber limit of the new instability is closed; the leading-order wavespeed has been determined and matching of the solution across

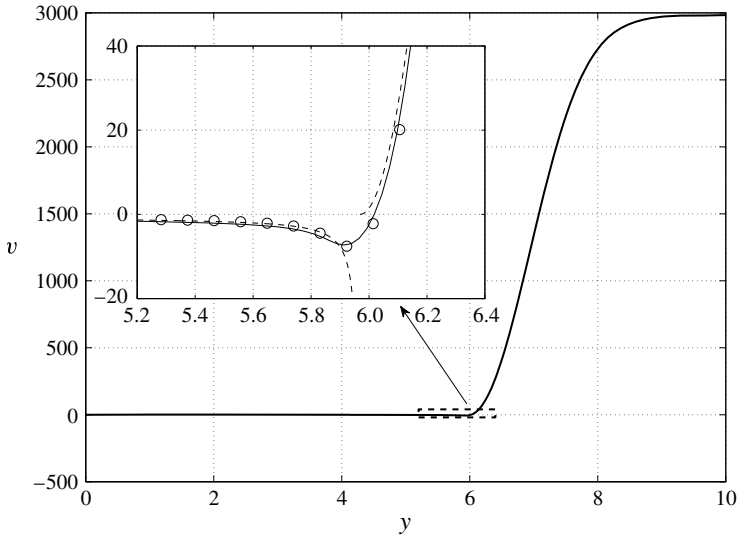

FIGURE 9. Numerical eigenfunction (——), leading-order asymptotic approximation in Region L, R (– – –) and Region I (○) of an inviscid low-wavenumber eigensolution of a disturbance to a typical overshoot boundary layer.

all the distinguished asymptotic regimes has been accomplished. This fact allows us to make some comparison between the predictions of our asymptotic analysis and the results of our numerical solution of the compressible Rayleigh equation. One such comparison is presented in figure 9 where we show the numerical solution and the first-order approximation (details of which can be found in appendix A). In making this comparison we have taken a value of c_1 from the numerically determined eigenvalue spectrum and chosen $n = 1/3$, a choice that matches well with the scaling of region I seen in the numerical solution. The close-up in the inner region I shows a comparison of the left L, inner I and right R regions with the full numerical solution. The comparison is very good, and provides strong validation of both the asymptotic analysis and numerical results.

6. Discussion and conclusion

The fact that self-similar compressible boundary layers often exist only under idealised conditions has long been accepted (see for example the discussions in Curle 1962; Stewartson 1964). Such models are however important in that they capture the dominant physics of the flow and using such self-similar flows as a proxy for full non-parallel boundary-layers allows us to explore the instability of such flows using classical techniques.

We have described a new two-dimensional mode of inviscid instability in such self-similar compressible boundary layers which exhibit a velocity overshoot. The overshoot results from the combined effect of a favourable pressure gradient and wall heating. Physically, the favourable pressure gradient acts across the entire boundary layer and serves to accelerate the fluid. Heating the wall serves to reduce the fluid density and so enhances the effect of the pressure gradient on the fluid's acceleration, hence leading to a region in the flow in which the streamwise velocity overshoots its free-stream value. There are two neutral points associated with this new mode of

instability. The first of these has a wavespeed equal to the maximum velocity in the boundary layer and occurs at zero wavenumber. The structure of the disturbance in this limit has been described using a small-α asymptotic analysis and this structure agrees well with the numerically-determined eigenfunctions. These asymptotic results presented in § 3 (and in appendix A) do not presume a self-similar flow, but simply one which manifests a velocity overshoot as a result of the aforementioned physics of streamwise acceleration and reduction in fluid density near the surface due to the surface heat transfer there. The second of these neutral points corresponds to a wave with a wavespeed such that there are two critical layers, neither of which corresponds to a generalised point of inflection. We conjecture that this neutral mode represents a wave trapped between the two critical layers, a conjecture that is supported by results from a fully viscous stability analysis in work by the present authors currently being prepared for publication. The fate of the inflectional neutral modes when the generalised point of inflection is in the overshoot region is unclear. In this case, there is a critical layer on either side of the velocity maximum and only one of these has the required generalised inflection point. We hope to be in a position to report on this problem in a future paper.

The new mode we have described will be one of the possible modes of instability in such flows, the others being the classical first mode and the higher 'Mack' modes (Mack 1984). In the large Reynolds number limit, these modes have similar growth rates and as such, one would expect that all three modes of instability are both observable and important, to perhaps varying degrees, in the ultimate fate of this class of compressible boundary layers. Future advances in experimental techniques for high speed flows, of the sort envisaged by Hirschel (1993), may be required if the role of this new mode of instability in the transition process of high speed flows is be fully understood.

Acknowledgements

A.P.T. gratefully acknowledges a University of Auckland Doctoral Scholarship. Thanks to Dr S. Stephen for drawing our attention to the HYTHIRM project.

Appendix A. Higher-order corrections

We present details of the analysis leading to the determination of the higher-order corrections to the eigensolution in the small wavenumber limit. We will consider the disturbance structure in the four regions separately.

A.1. *The first-order correction*

Region I

We develop subsequent correction terms to the leading-order solution by first considering region I, where the series expansion terms of v_{L0} as $y \to y_c^-$ suggests that a suitable expansion for $\hat{v}_I$ is

$$\hat{v}_I = \delta^2(v_{I0} + \delta v_{I1} + \delta^2 v_{I2} + \delta^3 \ln \delta v_{I3l} + \delta^3 v_{I3} + \cdots). \tag{A 1}$$

At $O(\delta^3)$, (5.6) yields

$$\mathscr{L}_I\{v_{I1}\} = D\bar{T}_c z - \frac{1}{6} D^3 \bar{u}_c z^6 \frac{\mathrm{d}}{\mathrm{d}z}\left(\frac{v_{I0}}{z^3}\right), \tag{A 2}$$

where the differential operator $\mathscr{L}_I$ was defined earlier. This equation admits the general solution

$$v_{I1} = \frac{2}{\lambda}B_4(z^2+\Gamma) - D\bar{T}_cB_3 + \frac{2}{3}\frac{D^3\bar{u}_c\bar{T}_c^2}{\Gamma^{3/2}}A_1z^3\left(\arctan\frac{z}{\sqrt{\Gamma}}+\frac{\pi}{2}\right). \tag{A 3}$$

As $z\to-\infty$ we have

$$v_{I1}\to\left[\frac{2}{\lambda}\left(B_4-\frac{1}{6}\frac{A_1D^3\bar{u}_c\bar{T}_c}{\lambda\Gamma}\right)\right]z^2+O(z^0). \tag{A 4}$$

In order to match with $\hat{v}_L$ the $O(z^2)$ term must vanish, serving to determine the constant B_4. The next term in this series expansion is now

$$v_{I1}\to\left[-B_3\frac{D\bar{T}_c}{\lambda}+\frac{4}{9}\frac{A_1D^3\bar{u}_c\bar{T}_c}{\lambda^2}\right]z^0+O(z^{-2}). \tag{A 5}$$

The z^0 term represents $\delta^3(y-y_c)^0$ and can match to the second term of v_{L0} in (5.11), which serves to determine the other integration constant B_3. Subsequent terms in the v_{I1} series expansion as $z\to-\infty$ need to be matched with subsequent correction terms in $\hat{v}_L$.

As $z\to+\infty$,

$$v_{I1}\to\left[\frac{\pi}{3}\frac{A_1D^3\bar{u}_c\bar{T}_c}{\Gamma^{3/2}\lambda^2}\right]z^3+O(z^0), \tag{A 6}$$

where the z^3 term represents $\delta^0(y-y_c)^3$ and matches trivially to the $(y-y_c)^3$ term of v_{R0}. The z^0 term is $O(\delta^3)$ in region R and suggests that a correction term of this magnitude is required in the expansion of $\hat{v}_R$.

Region L

The largest unmatched terms of $\hat{v}_I$ as $z\to-\infty$ are the z^{-3} term in v_{I0} and the z^{-2} term in v_{I1}, both of which are $O(\delta^3)$ in region L. Letting

$$\hat{v}_L=\delta^3(v_{L0}+\delta^2v_{L1}+\cdots) \tag{A 7}$$

and subsituting into (5.7) gives, at $O(\delta^3)$

$$D\left\{\mathscr{L}_O\{v_{L1}\}-\frac{c_1}{(\bar{u}-\bar{u}_{max})^2DI_L}Dv_{L0}-\frac{2M^2c_1}{(\bar{u}-\bar{u}_{max})DI_L}\mathscr{L}_O\{v_{L0}\}\right\}=0, \tag{A 8}$$

where we have defined

$$\mathscr{L}_O\{v\}=\frac{(\bar{u}-\bar{u}_{max})Dv-(D\bar{u})v}{\bar{T}-M^2(\bar{u}-\bar{u}_{max})^2}=D\left(\frac{v}{\bar{u}-\bar{u}_{max}}\right)(DI_L)^{-1}. \tag{A 9}$$

Solving for v_{L1} yields the general solution

$$\frac{v_{L1}}{\bar{u}-\bar{u}_{max}}=A_3I_L+A_4+A_1c_1\int_0^y\left[\frac{D\bar{u}I_L}{(\bar{u}-\bar{u}_{max})^2}+\frac{DI_L}{\bar{u}-\bar{u}_{max}}+\frac{2M^2}{\bar{u}-\bar{u}_{max}}\right]\mathrm{d}y, \tag{A 10}$$

where A_3 and A_4 are constants of integration. In order to satisfy the wall boundary condition, the constant A_4 must be zero. The two leading terms in the expansion as $y\to y_c^-$ match identically without additional constraints. The other integration constant A_3 appears in the $(y-y_c)^{-1}$ term of the expansion as $y\to y_c^-$, which is of size δ^2z^{-1} in Region I and hence needs to be matched with a z^{-1} term in v_{I2}, one that is yet to be determined.

Region R ($y \gg y_c$)

The largest unmatched terms of $\hat{v}_I$ as $z \to +\infty$ is the z^0 term in v_{I0}, which is $O\left(\delta^2\right)$ in region R. Extending the series to

$$\hat{v}_R = v_{R0} + \delta^2 v_{R1} + \delta^3 v_{R2} + \cdots \tag{A 11}$$

we obtain a similar equation to that of v_{L1} for v_{R1} namely.

$$D\left\{\mathscr{L}_O\{v_{R1}\} - \frac{c_1}{(\bar{u}-\bar{u}_{max})^2 D I_R} D v_{R0} - \frac{2M^2 c_1}{(\bar{u}-\bar{u}_{max}) D I_R}\mathscr{L}_O\{v_{R0}\}\right\} = 0. \tag{A 12}$$

This has the general solution

$$v_{R1} = C_3(\bar{u}-\bar{u}_{max}) I_R + C_4(\bar{u}-\bar{u}_{max}) - C_2 c_1, \tag{A 13}$$

where the constant C_3 must be zero to ensure the largest term is of the correct form to match with v_{I1}. As was the case with v_{L1}, the other constant of integration C_4 cannot be determined without reference to v_{I2}.

A.2. *The second-order correction*

Region I

At $O(\delta^2)$, (5.6) yields

$$\mathscr{L}_I\{v_{I2}\} = B_5 \frac{1}{2} D^2 \bar{T}_c z^2 - \frac{1}{6} D^3 \bar{u}_c z^6 \frac{\mathrm{d}}{\mathrm{d}z}\left(\frac{v_{I1}}{z^3}\right) - \frac{1}{24} D^4 \bar{u}_c z^8 \frac{\mathrm{d}}{\mathrm{d}z}\left(\frac{v_{I0}}{z^4}\right). \tag{A 14}$$

As $z \to -\infty$, the largest terms of v_{I2} are z^2, z^1 and z^{-1}, which in region L are $O(\delta^0)$, $O(\delta)$ and $O(\delta^3)$, respectively. The z^2 has no corresponding term to match to in region L and so must vanish, thus serving to determine one constant of integration. The other constant is set by matching the z^1 term with v_{L0}. The z^{-1} term is matched with the $(y-y_c)^{-1}$ term in v_{L1}, which yields $A_3 = 0$.

As $z \to +\infty$, v_{I2} has a z^4 term, a z^2 term and lower-order terms. The z^4 term is $O(\delta^0)$ and matches trivially with v_{R0}. The z^2 term is $O(\delta^2)$ and matching with the $(y-y_c)^2$ term in v_{R1} serving to determine C_4

$$C_4 = A_1 \frac{\pi}{12\lambda^4\sqrt{\Gamma}}(5D^3\bar{u}_c^2\bar{T}_c - 12\lambda D^3 \bar{u}_c D\bar{T}_c + 12\lambda^2 D^2 \bar{T}_c - 3\lambda D^4 \bar{u}_c \bar{T}_c). \tag{A 15}$$

Region R

In order to determine the eigenvalue correction term c_1, the solution for v_{R2} is required. The equation and solutions is the same as that for v_{R0}

$$v_{R2} = C_5(\bar{u}-\bar{u}_{max}) I_R + C_6(\bar{u}-\bar{u}_{max}), \tag{A 16}$$

however unlike v_{R0}, we keep the first term, which can be matched with the z^{-1} term in v_{I0}, and in fact $C_5 \equiv A_1$. As $y \to \infty$ we have

$$v_{R2} \to \left(\frac{1}{(1-\bar{u}_{max})^2} - M^2\right) y. \tag{A 17}$$

This term, when matched with the $\bar{y}$ term of $\hat{v}_F$, serves to determine c_1

$$c_1^3 = -\frac{\pi^2 \bar{T}_c^2 (1-\bar{u}_{max})^6}{2\lambda^3 (1 - M^2(1-\bar{u}_{max})^2)}. \tag{A 18}$$

Provided the maximum boundary-layer velocity is subsonic (in a Lees–Lin sense), the right-hand side of this expression is always positive and the solutions for c_1 consist of a positive real solution, and a complex conjugate pair whose real component is negative. It is this complex conjugate pair that corresponds to the new family of unstable modes. The nature of the inviscid stability equations is such that both the true inviscid eigenvalue and its conjugate are valid eigenvalues; the correct eigenvalue can only be determined by the high-*Re* limit of the viscous stability equations. We do not pursue this issue here but refer the reader to work currently being prepared for publication.

REFERENCES

BACK, L. H. 1969 Flow and heat transfer in laminar boundary layers with swirl. *AIAA J.* **7** (9), 1781–1789.

BAE, Y. Y. & EMANUEL, G. 1997 Tables for boundary-layer thicknesses of similar compressible laminar flow. *J. Mech. Sci. Technol.* **11** (4), 457–467.

BROWN, W. B. & DONOUGHE, P. L. 1951 Tables of exact laminar-boundary-layer solutions when the wall is porous and fluid properties are variable. *NACA Tech. Note* 2479.

COHEN, C. B. & RESHOTKO, E. 1955 Similar solutions for the compressible laminar boundary layer with heat transfer and pressure gradient. *NACA Tech. Rep.* 1293.

CURLE, N. 1962 *The Laminar Boundary Layer Equations*. Oxford University Press.

DENIER, J. P., DUCK, P. W. & LI, J. 2005 On the growth (and suppression) of very short-scale disturbances in mixed forced-free convection boundary layers. *J. Fluid Mech.* **526**, 147–170.

DENIER, J. P. & MUREITHI, E. W. 1996 Weakly nonlinear wave motions in a thermally stratified boundary layer. *J. Fluid Mech.* **315**, 293–316.

FEDOROV, A. V. 2011 Transition and stability of high-speed boundary layers. *Annu. Rev. Fluid Mech.* **43** (1), 79–95.

FU, Y., HALL, P. & BLACKABY, N. 1993 On the Görtler instability in hypersonic flows: Sutherland law fluids and real gas effects. *Proc. R. Soc. Lond.* A **342**, 325–377.

GIBSON, D. W., SPISZ, T. S., TAYLOR, J. C., ZALAMEDA, J. N., HORVATH, T. J., TIETJEN, A. B., TACK, S. & BUSH, B. C. 2010 HYTHIRM radiance modeling and image analyses in support of STS-119, STS-125 and STS-128 space shuttle hypersonic re-entries. *AIAA Paper* 2010-245.

HIRSCHEL, E. H. 1993 Hot experimental technique: a new requirement of aerothermodynamics. In *New Trends in Instrumentation for Hypersonic Research* (ed. D. L. Dwoyer & M. Y. Hussaini), NATO ASI Series, vol. 224, pp. 25–39. Springer.

LEES, L. & LIN, C. C. 1946 Investigation of the stability of the laminar boundary layer in a compressible fluid. *NACA Tech. Note* 1115.

LI, T. Y. & NAGAMATSU, H. T. 1955 Similar solutions of compressible boundary layer equations. *J. Aeronaut. Sci.* **22**, 607–616.

MACK, L. M. 1975 Linear stability theory and the problem of supersonic boundary layer transition. *AIAA J.* **13**, 278–289.

MACK, L. M. 1984 Special course on stability and transition of laminar flow. *AGARD Report* 709.

MACK, L. M. 1987 Review of linear compressible stability theory. In *Stability of Time Dependent and Spatially Varying Flows* (ed. D. L. Dwoyer & M. Y. Hussaini), pp. 164–187. Springer.

MALIK, M. R. 1990*a* Numerical methods for hypersonic boundary layer stability. *J. Comput. Phys.* **86** (2), 376–413.

MALIK, M. R. 1990*b* Prediction and control of transition in supersonic and hypersonic boundary layers. *AIAA J.* **27**, 1487–1493.

MASAD, J. A., NAYFEH, A. H. & AL-MAAITAH, A. A. 1992 Effect of heat transfer on the stability of compressible boundary layers. *Comput. Fluids* **21**, 43–61.

MCLEOD, J. B. & SERRIN, J. 1968*a* The behaviour of similar solutions in a compressible boundary layer. *J. Fluid Mech.* **34** (02), 337–342.

MCLEOD, J. B. & SERRIN, J. 1968*b* The existence of similar solutions for some laminar boundary layer problems. *Arch. Rat. Mech. Anal.* **31**, 288–303.

MORKOVIN, M. V. & RESHOTKO, E. 1990 Dialogue on progress and issues in stability and transition research. In *Laminar-Turbulent Transition* (ed. R. Eppler & H. Fasel), pp. 3–29. Springer.

MUREITHI, E. W., DENIER, J. P. & STOTT, J. 1997 The effect of buoyancy on upper-branch Tollmien–Schlichting wares. *IMA J. Appl. Maths* **58**, 19–50.

NEELY, A. J., DASGUPTA, A. & CHOUDHURY, R. 2014 A new method for prescribing non-uniform wall temperatures on wind tunnel models. In *Proceedings of the 19th Aust. Fluid Mech. Conference*, Melbourne, Australia, 8–11 December, RMIT University.

RESHOTKO, E. & BECKWITH, I. E. 1957 Compressible laminar boundary layer over a yawed infinite cylinder with heat transfer and arbitrary Prandtl number. *NACA Tech. Note* 3986.

SCHMID, P. J. & HENNINGSON, D. S. 2001 *Stability and Transition in Shear Flows*. Springer.

STEINRÜCK, H. 1994 Mixed convection over a cooled horizontal plate: non-uniqueness and numerical instabilities of the boundary-layer equations. *J. Fluid Mech.* **278**, 251–265.

STEWARTSON, K. 1964 *The Theory of Laminar Boundary Layer in Compressible Fluids*. Oxford University Press.

ZAMELDA, J. N., HORVATH, T. J., TOMEK, D. M., TIETJEN, A. B., GIBSON, D. M., TAYLOR, J. C., TACK, S., BUSH, B. C., MERCER, C. D. & SHEA E., J. 2010 Application of a near infrared imaging system for thermographic imaging of the space shuttle during hypersonic re-entry. *AIAA Paper* 2010-244.